Evidence of 210Po on Martian dust at Meridiani Planum

Pierre-Yves Meslin, Jean-Christophe Sabroux, Lionel Berger, Jean-François Pineau, Eric Chassefière

Evidence of ^{210}Po on Martian dust at Meridiani Planum

Pierre-Yves Meslin,[1] Jean-Christophe Sabroux,[1] Lionel Berger,[1] Jean-François Pineau,[2] and Eric Chassefière[3]

Received 31 January 2006; revised 4 April 2006; accepted 15 May 2006; published 21 September 2006.

[1] Since the Surveyor and Apollo missions and up to the recent Lunar Prospector mission, ^{222}Rn and ^{210}Po have been key isotopes for understanding gas release events and their spatial and temporal variations on the Moon. Comparatively, these isotopes have drawn much less attention on Mars, if any, despite the wealth of information it could bring on the uppermost meters of the regolith, the exchange of volatiles at the surface, and the atmospheric aerosol cycle. Here we present a statistical analysis of the high-energy end of alpha spectra obtained by the alpha particle X-ray spectrometer onboard Mars Exploration Rover Opportunity and report evidence of ^{210}Po, a decay product of ^{222}Rn, attached to atmospheric dust. The ^{210}Po surface activity on rocks and soils at the landing site is lower than 3.1×10^{-4} Bq cm^{-2}, but analysis of spectra obtained on the dust capture magnet reveals a ^{210}Po activity of $(4.6 \pm 2.4) \times 10^{-3}$ Bq cm^{-2} ($\pm 2\sigma$). This difference is due to the very low dust cover index at the landing site. Owing to frequent dust devils, regional and global dust storms that mobilize substantial amounts of dust and homogenize the dust surface layer, we infer that the global average ^{222}Rn exhalation rate is significantly greater on Mars than on the Moon. This comparison supports the hypothesis that on Mars, radon emanation could be comparatively enhanced by the presence of water in the surficial soil. Analysis of atmospheric spectra yields a radon activity upper limit of 16 ± 5 Bq m^{-3} during nighttime at the landing site.

Citation: Meslin, P.-Y., J.-C. Sabroux, L. Berger, J.-F. Pineau, and E. Chassefière (2006), Evidence of ^{210}Po on Martian dust at Meridiani Planum, *J. Geophys. Res.*, *111*, E09012, doi:10.1029/2006JE002692.

1. Introduction

[2] The alpha particle X-ray spectrometer (APXS) onboard both Mars Exploration Rovers (MER) Spirit and Opportunity was primarily designed to measure the concentration of virtually all major elements ($Z \leq 40$, except H and He) at the surface of Martian rocks and soils. This technique has been successfully used on Mars since the Pathfinder mission [*Rieder et al.*, 1997]. Most MER results published so far pertain to the spectrometer X-ray mode of operation with special emphasis on volatile elements such as sulfur, chlorine and bromine [*Gellert et al.*, 2004; *Rieder et al.*, 2004]. In its alpha mode, however, the spectrometer is more specifically sensitive to lighter elements, such as carbon and oxygen. The spectrometer measurement principle consists of bombarding targets with alpha particles emitted by a radioactive source of high specific activity (^{244}Cm, in the GBq activity range) and measuring the energy of backscattered particles, whose energy distribution is predicted by the Rutherford backscattering (RBS) theory. The alpha detectors onboard the MER are thoroughly described by *Rieder et al.* [2003]. Their cutoff energy was set to about 6 MeV, enabling them to measure backscattered alpha particles emitted by the curium source (5.805 and 5.763 MeV, reduced to ~5.17 MeV by a 2.5 μm titanium foil). It turns out that the upper part of this energy range (Figure 1a) also encompasses emission lines from several natural alpha-emitting radionuclides. Thus we have investigated into the possible contribution of natural radioactive sources to alpha spectra, namely of ^{210}Po and ^{222}Rn. The presence of these decay products of ^{238}U, in significant amounts at the Martian surface, is indeed made possible owing to exhalation of ^{222}Rn from the subsurface (Figure 2).

[3] Polonium 210 originates from the radioactive decay of ^{210}Pb, which has a half-life of 22.3 years. Polonium 210 itself has a half-life of 138 days and disintegrates into the stable end product ^{206}Pb by emission of a 5.304 MeV alpha particle. Special circumstances make its detection possible by Opportunity's APXS detector. We first looked at spectra obtained by Pathfinder's APXS, but the thin aluminum foil that was originally covering the ^{244}Cm sources to avoid contamination of samples by recoil sputtering of the source material, and to avoid resonance in the ^{12}C(α, α')^{12}C reaction [*Rieder et al.*, 2003], was later removed on the flight version, leading to an important noise level below 5.8 MeV, i.e., over the range of energies of interest. Fortunately, a 2.5 μm titanium foil was present on the MER APXS curium sources, removing noise from recoil sputtering and

[1] Institut de Radioprotection et de Sûreté Nucléaire, Centre de Saclay, Gif-sur-Yvette, France.
[2] ALBEDO Technologies, Razès, France.
[3] Service d'Aéronomie, Institut Pierre–Simon Laplace, Paris, France.

0148-0227/06/2006JE002692

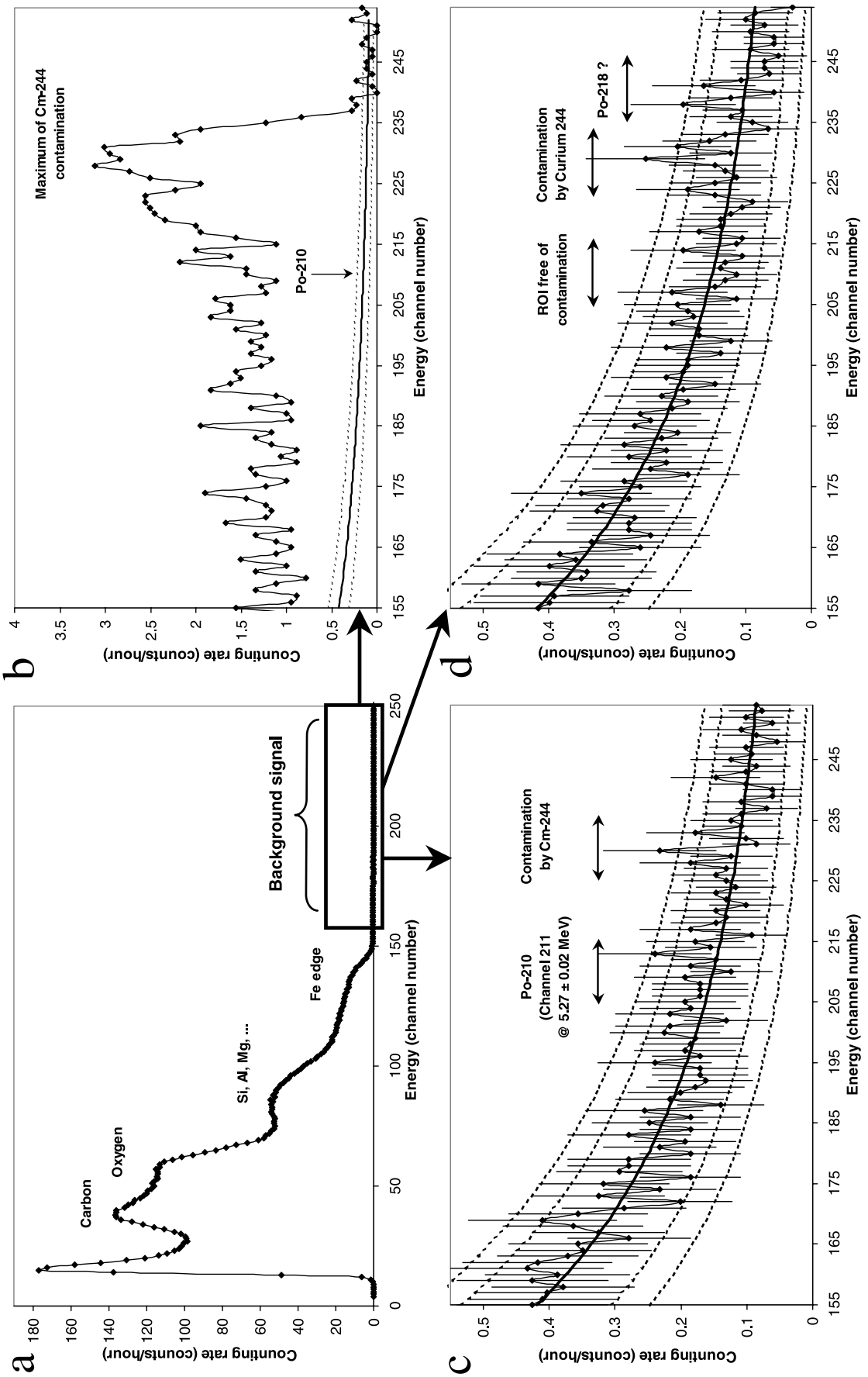
a
Counting rate (counts/hour)
Energy (channel number)
Carbon
Oxygen
Si, Al, Mg, ...
Fe edge
Background signal
b
Maximum of Cm-244 contamination
Po-210
c
Po-210 (Channel 211 @ 5.27 ± 0.02 MeV)
Contamination by Cm-244
d
ROI free of contamination
Contamination by Curium 244
Po-218 ?

Figure 1

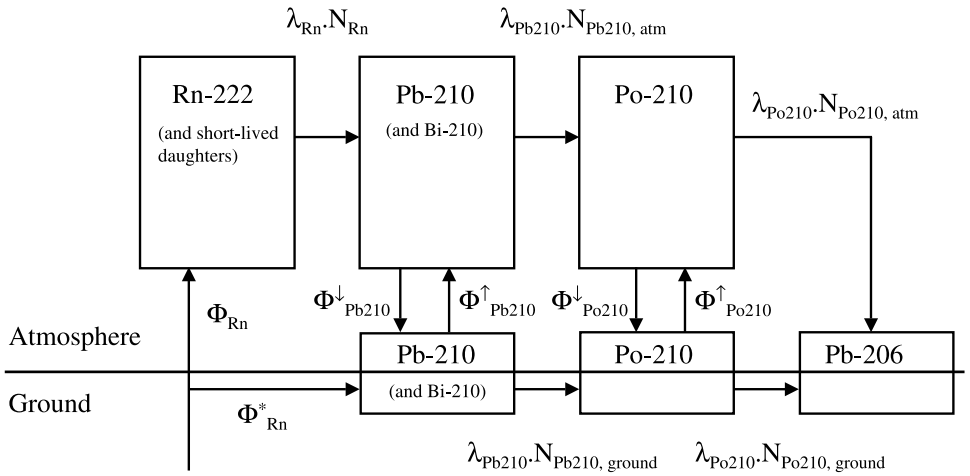

Figure 2. Sketch of the box model relating atmospheric and surface reservoirs of ^{222}Rn and its decay products on Mars. Arrows are associated with source and sink terms. Short-lived daughters (^{218}Po, ^{214}Pb, ^{214}Bi, and ^{214}Po) and ^{210}Bi are not represented.

lowering the energy of backscattered alphas. This foil turned out to be particularly efficient on Opportunity's APXS for the first 168 Martian solar days (or sols, 1 sol being equal to 24.65 hours) of operation, after which a physical degradation became noticeable. Spectra from Spirit's APXS show parasite signals in that energy range from almost the first operation sols. We therefore focused our analysis on spectra (raw uncalibrated data) acquired by Opportunity for the first 168 sols of operation [*Rieder and Gellert*, 2004]. The list of targets and their type is summarized in Table 1.

2. Procedure

2.1. General Description

[4] The first steps consisted of localizing the channel corresponding to the energy of ^{210}Po alpha particles on APXS spectra and to determine the in situ energy resolution of the detector, in order to estimate the width of the energy window possibly affected by the presence of a ^{210}Po source on the surface of rocks. Then, a statistical analysis has been carried out to see whether a signal was emerging from the background noise at these energies. The radionuclide activity has been derived from the measured signal by calculating the geometrical detection efficiency of the detector.

2.2. Energy Calibration of APXS Spectra

[5] We carried out an a posteriori calibration of APXS spectra (256 channels) by looking at conspicuous features of the spectra at different energies, and by comparison with results from the spectrum simulation software SIMNRA 5.02 [*Mayer*, 1997]. The features used as reference were: oxygen and carbon peaks; silicon, iron and argon signal edges on solid and atmospheric targets, respectively; gold peak, present when the door of the APXS sensor head was closed for calibration purpose (on sols 12 and 52); and ^{244}Cm peak present after sol 175 because of foil's degradation. Channel numbers were retrieved from raw data and their corresponding energy was obtained from simulation with SIMNRA 5.02, taking into account the slight energy attenuation across the 3 cm working distance of the instrument. The instrument calibration turned out to be very linear (Figure 3) and showed a very good stability from one sol to another. Slight corrections were made when needed to compensate for changes in working distance possibly combined with pressure/temperature variations (simple shift of the spectra toward lower energies), as well as for slight calibration drifts, by checking and adjusting the position of specific features shown in Figure 3. Sols 54, 70 and 122 presented wide variations and were therefore discarded.

[6] Finally, we were able to predict that a monoenergetic source of alpha radiation at 5.304 MeV (characterizing unambiguously ^{210}Po) would produce a peak centered at channels 210–211, after attenuation by the 3 cm thick layer of CO_2 at 2×10^{-5} g cm^{-3}. The uncertainty is about ±30 keV (1 to 2 channels), which is of the same order as possible drifts due to changes in working distance combined with pressure/temperature variations. However, given the detector's resolution (≈250 keV at 5.8 MeV, see section 2.3) and the low

Figure 1. Spectra obtained by the APXS alpha particles detector. (a) Spectrum of a typical Martian rock, showing the region of interest for the present study (4.0–6.2 MeV). (b) Spectrum obtained over the energy range (4.0–6.2 MeV) from sol 175 to sol 180, showing evidence of a contamination by the curium source, peaking around channel 230. Solid and dashed lines show the signal level before contamination and its confidence interval. (c) Gross signal (S + B) integrated over a period of time of 129 hours, with power law fit (thick solid line) and 2σ and 3σ detection thresholds obtained from the fit (dashed lines). (d) Blank signal (B) integrated over a period of time of 123 hours, with the same fit and 2σ and 3σ detection thresholds as Figure 1c. No peak is present in the region of interest (ROI): any kind of contamination seems precluded. Error bars are ±2σ. The contribution of ^{218}Po on RAT spectra is proposed as a possible explanation for the presence of two anomalies around channel 239 due to electrostatic charging of the abraded surface.

Table 1. List and Types of Targets of the APXS for the First 168 Operation Sols of Opportunity

	Gross Signal		Blank		
	Rock/Soil/Wind streak	Magnet	RAT	Trench	Atmosphere
SOL	11, 15, 23, 29, 40, 41, 43, 46, 48, 49, 50, 52, 53, 54, 60, 66, 80, 91, 100, 106, 123, 142, 166	53, 168	25, 30, 31, 36, 45, 48, 68, 81, 87, 91, 108, 139, 145, 147, 149, 153, 155, 162	25, 81, 91	7, 79
Integration time	119 hours	10.3 hours	123 hours		18.5 hours

signal-to-noise ratio conditions, and because of possible variations of the amplifier's gain, any peak is expected to be strongly distorted rather than well resolved, and a statistical analysis is therefore more appropriate than a classical spectroscopic approach based on analytic functions fitting routines.

[7] A more local energy calibration was also obtained by considering only the gold and curium peaks, at channels 175 and 230, that is by considering only the last two points of the calibration curve (Figure 3). The position of a hypothetical ^{210}Po peak remains almost unchanged (centered at channel 209).

2.3. Determination of the in Situ Detector Energy Resolution

[8] By looking at the ^{244}Cm contamination peak measured after sol 168 (Figure 1b), one can estimate the full-width-half-maximum (FWHM) at 5.8 MeV to be about 11 channels, or ≈250 keV. The long tail toward low energies of this peak is probably due to spatially dispersed contamination resulting in a wide range of incidence angles of ^{244}Cm alpha particles. A good way of estimating the one half FWHM is thus to consider only the upper half portion of the peak. This resolution takes into account the broadening due to the 3 cm of CO_2 crossed by the alpha particles (most sputtered ions are assumed to be deposited onto the target surface). However, it also encompasses the broadening caused by the presence of 2 alpha decay lines of ^{244}Cm, 40 keV apart (5.805 and 5.763 MeV), which would not affect the resolution of a ^{210}Po peak. The absolute energy resolution at 5.3 MeV is also expected to be slightly better than the resolution at 5.8 MeV.

[9] Another way of estimating the energy resolution of the detector is to look at the Au peak of the calibration target (Figure 4). Its FWHM is about 11 channels, but this includes additional straggling caused by alpha particles traveling back and forth through the 3 cm working distance and through the target's thickness.

[10] Finally, we chose a FWHM of 11 channels, or 250 keV, to take into account possible variations of the working distance.

2.4. Signal Statistical Analysis

[11] The procedure first consisted of comparing dust-covered versus uncovered targets. Indeed, ^{210}Po is supposed to cover more or less homogeneously the whole planet, its long-lived parent ^{210}Pb being deposited onto the surface with atmospheric dust. Because of the low surface activity expected, we summed up a large number of spectra, obtained from sol 11 to sol 168 on dusty rocks, soils, wind streaks, as well as on the so-called capture magnet, aimed at collecting airborne magnetic dust [*Madsen et al.*, 2003]. Precious information on background noise was separately obtained from measurements carried out in holes drilled in rocks by the rock abrasion tool (RAT) and in trenches dug by the rover wheel. Indeed, no signal from ^{210}Po is expected

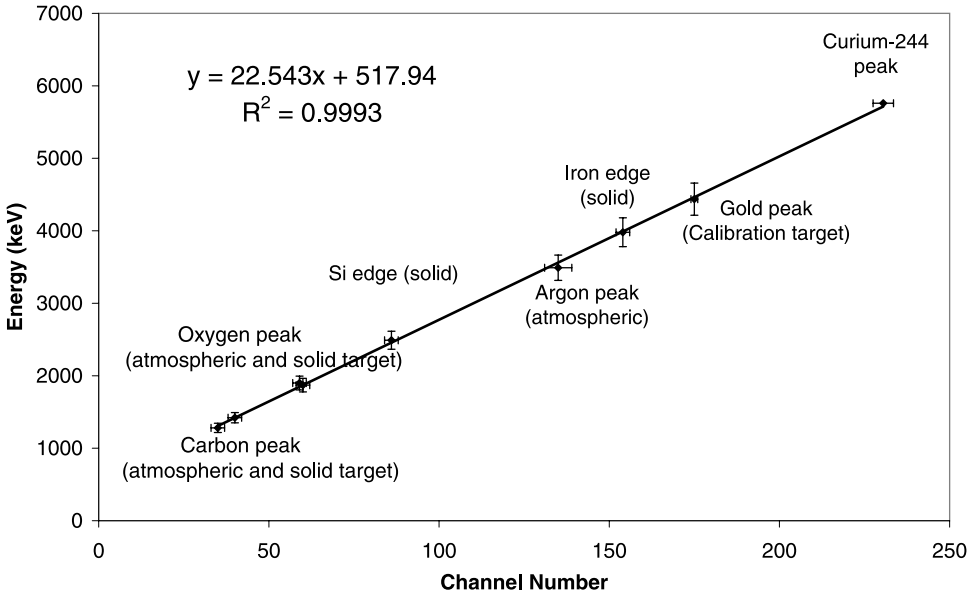

Figure 3. Calibration curve: energy of incident particles versus channel number of the multichannel analyzer (MCA).

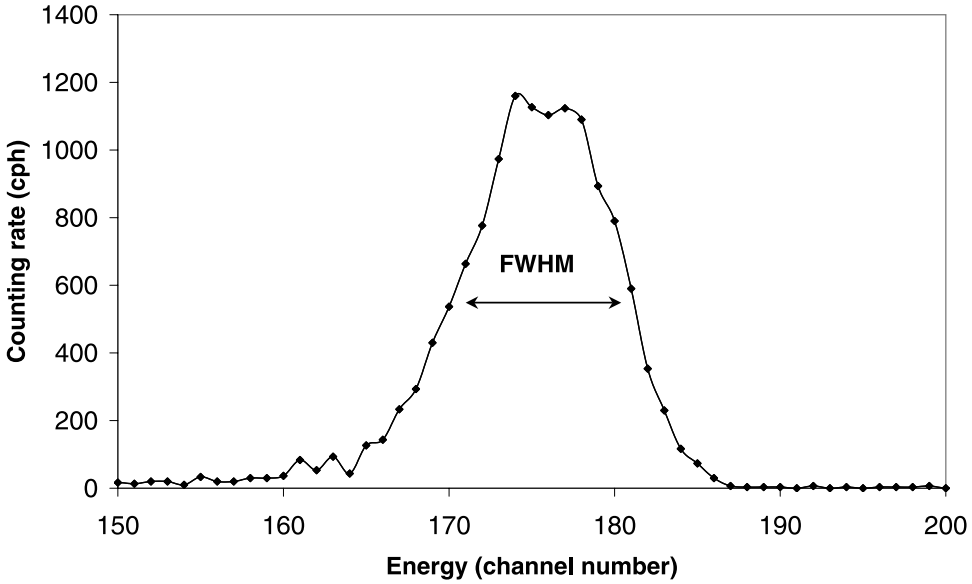

Figure 4. Gold peak of the calibration target, measured by RBS when the door of the APXS sensor is closed. Its FWHM is about 11 channels, but this includes additional straggling caused by alpha particles traveling back and forth in the Martian atmosphere through the 3 cm working distance and through the target's thickness.

on these spectra, the uranium-supported fraction of ^{210}Po present in the target material (i.e., ^{210}Po in equilibrium with its parent ^{238}U within the mineral grains) being negligible. Thereafter, we call "blank" the sum of (RAT + Trenches) measurements. Finally, we analyzed Opportunity's data through two different approaches, as *Gorenstein and Bjorkholm* [1972] did in their analysis of the ^{210}Po signal coming from the surface of the Moon during the Apollo 15 mission.

[12] The first method consists of comparing the signal at the energy of interest with the background level given by neighboring channels, fitted over the whole energy range. The advantage of this method is its robustness with respect to an episodic and general increase of the background noise, since such an increase will also raise the fit. The gross signal is plotted in Figure 1c, together with statistical error bars, signal fit, and 2σ and 3σ detection thresholds calculated from the fit. Statistical anomalies appear at channel 213 and around channel 230. The presence of the latter ones probably results from the onset of recoil-sputtering contamination, which only bursts significantly after sol 168. Indeed, a closer look at spectra acquired from sols 175 to 180 shows that contamination by the curium source also peaks at these energies (Figure 1b). Furthermore, this peak is also visible on the blank, contrary to the peak at channel 213 (Figure 1d). The difference between the gross signal and its fit is plotted in Figure 5a. An integration of the net signal over an energy width of 11 channels (the resolution of the detector) brings out two statistical anomalies at channels 210 and 230, above the 95% and 97.5% detection thresholds, respectively (Figure 5b). We therefore conclude with a very safe confidence level that the ^{210}Po and ^{244}Cm signals are present.

[13] The second method consists of looking for an increase of the signal in the region of interest between the gross signal (S + B), and the blank signal (B). The blank spectrum is shown in Figure 1d. It can be seen that the noise level is particularly low in the region of interest, i.e., in the range [5.1 MeV to 5.3 MeV]. This is crucial to confirm the presence of a ^{210}Po signal: indeed, we looked at other possible reasons for the presence of a peak in these channels, such as sum peak, pollution of the detector by recoil sputtering, pollution by exogenic ^{210}Po (the alpha spectrometer onboard *Apollo* 15 was polluted with ^{210}Po deposited on the detector during prelaunch lab calibration tests) or by other radionuclides (including ^{240}Pu, the decay product of ^{244}Cm, at 5.168 and 5.124 MeV, other transuranian isotopes, or elements of the ^{232}Th series). However, given the low counting rate, a sum peak is excluded, and the half-life of ^{240}Pu is too long to yield any observable signal. Alpha particles emitted by the decay products of ^{220}Rn, from the ^{232}Th series, have energies above the cutoff energy. Moreover, a backscattered signal cannot produce a peak higher than the emission energy of 5.17 MeV, i.e., higher than channel 207, unless there is a wide calibration drift. Above all, if any kind of contamination or parasite signal were present constantly, it would have appeared on the blank spectrum as well (Figure 1d). Comparison between the blank and the fit does not reveal any anomaly other than the slight ^{244}Cm contamination (Figure 6). Furthermore, we checked the time evolution of the gross signal to ensure that no punctual burst occurred in the region of interest, possibly stemming from instrumental failure. The signal level in this region was found to be significantly larger only on the capture magnet, as expected (see section 3.1). Again, integrating the net signal over a width of 11 channels reveals the presence of a statistical anomaly at the energy of ^{210}Po at the 97.5% detection threshold (Figure 5d).

2.5. Detection Threshold

[14] There is an extensive set of decision rules to decide a posteriori whether a signal has been detected or not, but not

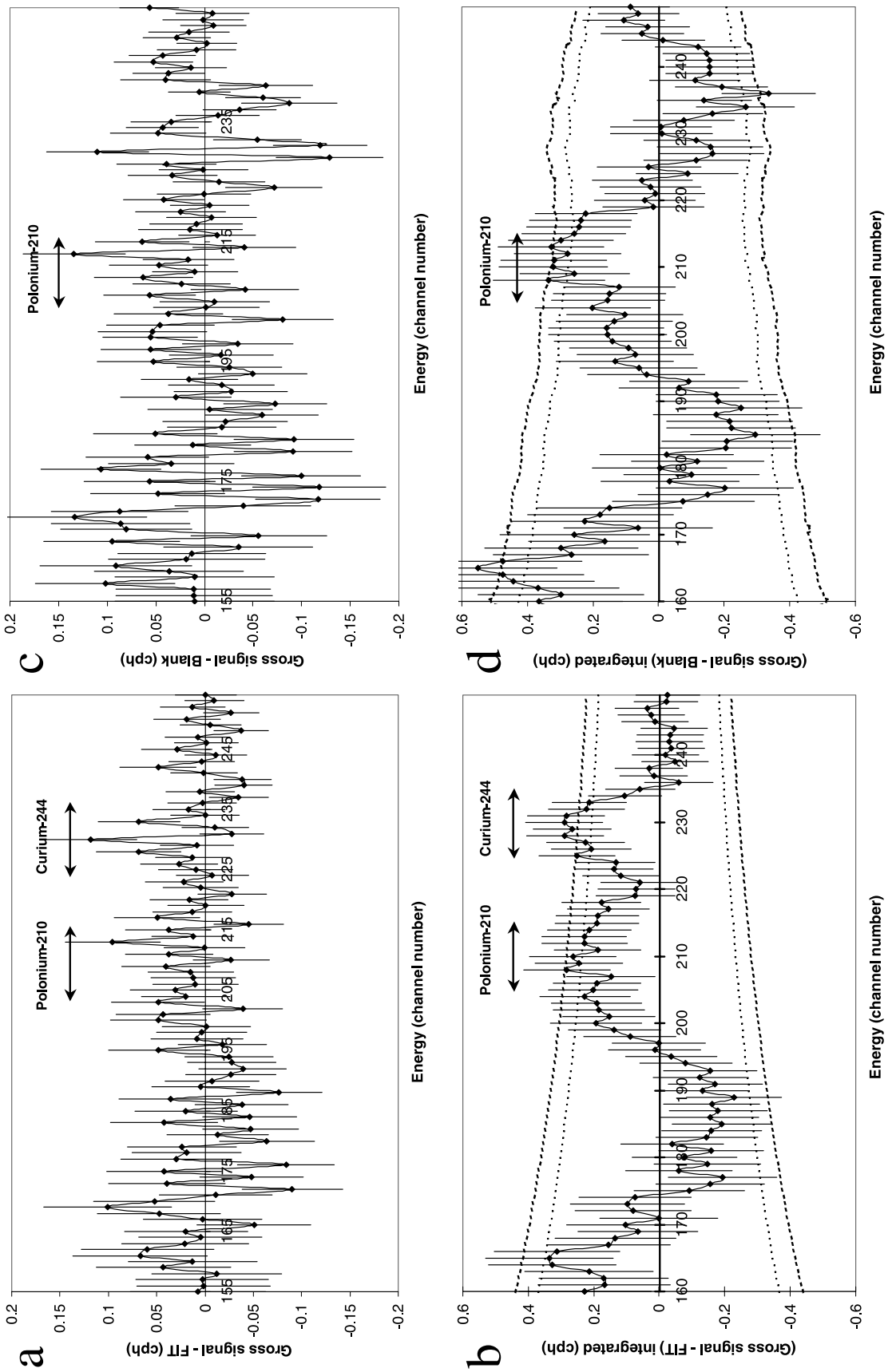
a
Gross signal - FIT (cph)
Energy (channel number)
Polonium-210
Curium-244
b
(Gross signal - FIT) integrated (cph)
Energy (channel number)
Polonium-210
Curium-244
c
Gross signal - Blank (cph)
Energy (channel number)
Polonium-210
d
(Gross signal - Blank) integrated (cph)
Energy (channel number)
Polonium-210

Figure 5

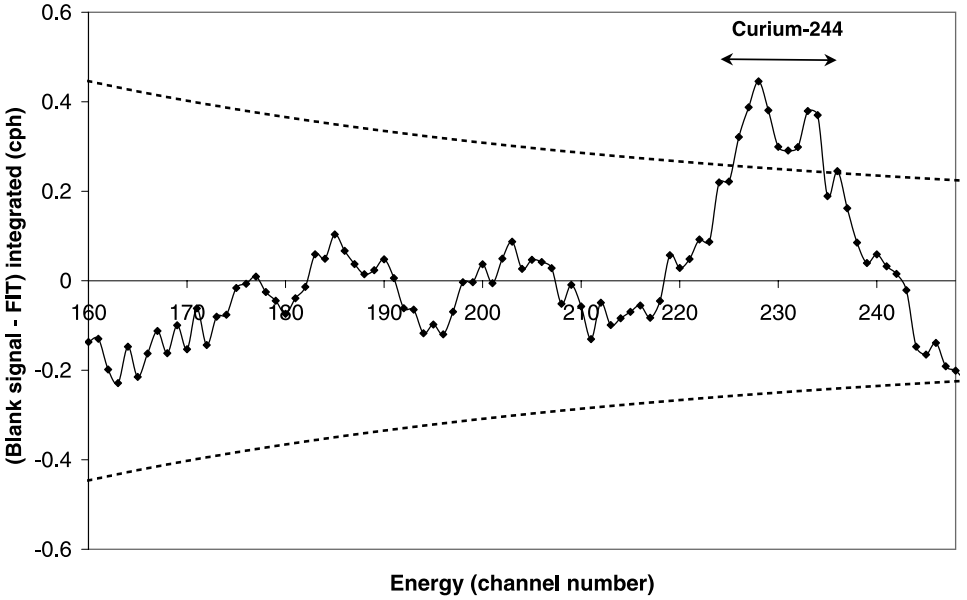

Figure 6. Difference between the blank signal (Figure 1d) and the fit, integrated over a width of 11 channels. The dashed lines represent the one-sided 95% detection threshold. There is no anomaly besides the ^{244}Cm peak at channel 230.

all of them are reliable under low-level counting rate conditions. *Strom and MacLellan* [2001] describe and compare eight decision rules for low-level radioactivity counting and show that, for a probability α = 5% (2%) of making an error of the first kind (i.e., in our case, deciding that ^{210}Po is present when it is not), the so-called McCroan, Nicholson D_1, Nicholson D_3, Turner/Altshuler&Pasternak and Stapleton's decision rules all coincide for a mean background signal greater than 2 (respectively 6) counts, in the "paired blank" case (equal background and gross count times). In the present case, after integrating the signal over 11 channels, we have a background of about 200 counts in the region of interest, so we can use any of these rules. The detection threshold, sometimes called Critical Level [*Currie*, 1968], L_C, was finally calculated according to McCroan's formula (recommended in ISO standard 11929-1:2000 "Determination of the detection limit and decision threshold for ionizing radiation measurements—Part I", available at http://www.iso.org):

$$L_C = \frac{1}{2t_B} k_{1-\alpha}^2 \left(1 + \sqrt{1 + \frac{4B}{k_{1-\alpha}^2} \left(1 + \frac{t_B}{t_{S+B}} \right)} \right) \qquad (1)$$

where B is the measured blank signal (in counts), t_B and t_{S+B} the integration times of the blank and gross signals, respectively, and $k_{1-\alpha}$ the $(1-\alpha)$ fractile of a standardized normal distribution, defined as $P(X < k_{1-\alpha}) = 1-\alpha$, where $P(X < k_{1-\alpha})$ is the probability that the random variable X following a standardized normal distribution is lower than $k_{1-\alpha}$. For a probability α = 5% (2.5%) of making an error of the first kind: $k_{1-\alpha}$ = 1.645 (respectively 1.960). For the first approach, B was estimated from the fit of the gross signal, by integrating the fit below the peak of ^{210}Po. In that first case, we had: t_{S+B} = 129 hours and t_B = 252 hours (see section 2.6). For the second approach, B was directly estimated from the measured blank signal. In that second case, we had: t_{S+B} = 129 hours and t_B = 123 hours (thus this is almost the "paired blank" case studied by *Strom and MacLellan* [2001]).

[15] However, it should be pointed out that all the above mentioned decision rules assume that the background variance is consistent with that of a Poisson process, i.e., that it is equal to B. To ensure that this assumption holds, we have compared the standard deviation s of a subset of 157 1-hour spectra (the spectra stored in the APXS memory buffers can have different integration times, from a few minutes to 2 hours, but for the present purpose, we need to analyze a population of spectra with same integration time, so the whole population could not be conside red) with the standard deviation σ of a Poisson process, to see if they were consistent. Each 1-hour spectrum was integrated over the range [channel 155; channel 254],

Figure 5. Net signal ($\pm\sigma$). (a) Difference between the gross signal (Figure 1c) and the fit. (b) Each data point represents the integration of the net signal (Figure 5a) over an energy width of 250 keV ([−5; +5] channels) centered around that point. This width corresponds to the detector's energy resolution. (c) Difference between the gross signal (Figure 1c) and the blank (Figure 1d). (d) Each data point represents the integration of the net signal (Figure 5c) over an energy width of 250 keV. Solid squares and dashed lines represent the one-sided 95% and 97.5% detection thresholds, respectively. Below channel 170, RAT and superficial spectra tend to differ, probably owing to the presence of trace elements heavier than Fe, in particular Ni, Zn, and Br, whose abundance can differ depending on the type of target [*Gellert et al.*, 2004; *Rieder et al.*, 2004]. It should be noted that the ubiquitous ^{244}Cm peak disappears when the blank signal is subtracted.

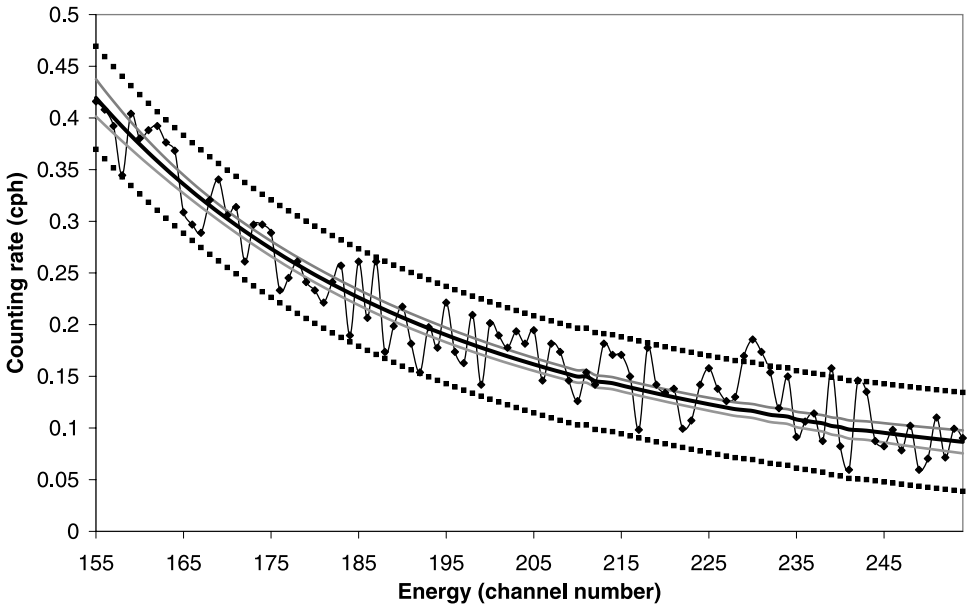

Figure 7. Alpha spectrum obtained after 252 hours of integration (diamonds), together with power law fit (black solid line), 95% prediction interval (squares), and 95% confidence interval (gray solid lines) of the fit. The 95% prediction interval is defined as the Y range for a given X where there is a 95% probability that the next experiment's Y value will occur, based upon the fit of the experiment's data. The 95% confidence interval is defined as the Y range for a given X that has a 95% probability for containing the true Y value. Two peaks are still above the 95% prediction interval (at channels 230 and 239), corresponding to the ^{244}Cm signal and possibly to a ^{218}Po signal. The peak of ^{210}Po vanished in the fluctuations of the background signal.

which is essentially the range affected by the background noise only. We obtained an average background $\overline{b}$ = 19.38 counts per hour (cph), with an estimated standard deviation s = 4.43 cph. A pure Poisson process would have yielded a standard deviation $\sigma = \sqrt{\overline{b}}$ = 4.40 cph. Using a χ^2 test with N − 1 = 157 − 1 = 156 degrees of freedom, we find $(s/\sigma)^2$ to be nonsignificant (p = 0.44, p = 0.50 corresponding to the least significant result achievable), so the background signal is most likely governed by a Poisson process and the use of formula (1) is justified.

2.6. Fitting Procedure

[16] The first approach was based on the comparison between the gross signal and its fit over a rather large energy range (about hundred data points). This fit was obtained by fitting the signal above channel 155 after summation of all spectra (Rocks + Soils + RAT + Trenches), in order to improve its accuracy (total integration time of 129 + 123 = 252 hours). The contribution of the ^{244}Cm and ^{210}Po signals was removed prior to fitting. The best fit was found to be the following power law: $FIT(E) = 0.0225 + 5.188 \times 10^7 \times E^{-3.706}$, where E is the energy, expressed in channel number (see Figure 7). The normality of the residuals was checked on a stabilized normal probability plot, ensuring the goodness of the fit. We also performed a chi-square goodness of fit test to detect any departure of the residuals distribution from a Gaussian distribution (see, for example, *Soong* [2004] for a description of this test). The null hypothesis H_0 = "the residuals are derived from a Gaussian distribution" can be accepted at the 5% significance level, which means that the difference between the residuals and any random sample from a Gaussian distribution is not significant.

3. Quantitative Results

3.1. Polonium 210 Signal

[17] Comparison between dust-covered and dust-uncovered targets revealed the presence of ^{210}Po on Martian dust. However, the targets do not contribute equally to the ^{210}Po signal. The signal measured on rocks and soils only (t_{S+B} = 119 h, S + B = 1.76 cph, B_{mean} = 1.64 cph, S_{mean} = 0.12 cph) is below the detection threshold (L_{Cmean} = 0.26 cph), while the signal measured on the capture magnet (t_{S+B} = 10.3 h, S + B = 4.10 cph, B_{mean} = 1.69 cph, S_{mean} = 2.41 cph), well above L_{Cmean} = 0.70 cph, L_C being a function of t_{S+B}, according to equation (1), accounts for most of the net signal. This discrepancy comes from the fact that Opportunity's landing site shows among the lowest dust cover indices on Mars [*Ruff and Christensen*, 2002; *Soderblom et al.*, 2004; *Catling*, 2005], whereas the magnet is almost fully covered with atmospheric dust [*Bertelsen et al.*, 2004]. Figure 8 clearly shows the spectral signature of ^{210}Po attached to dust particles collected by the strong magnet. Table 2 summarizes quantitative results obtained for the two different approaches described above. The uncertainty around the mean net signal was calculated from:

$$\sigma_{\overline{S}} = \sqrt{\sigma^2_{S+B} + \frac{1}{4}.\sigma^2_{B_1} + \frac{1}{4}.\sigma^2_{B_2}} \qquad (2)$$

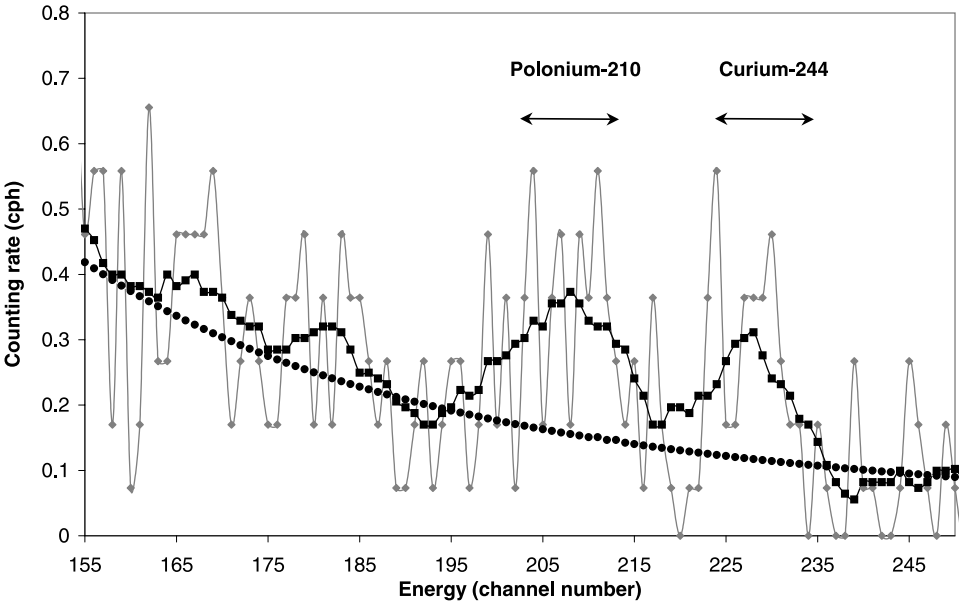

Figure 8. Alpha spectrum of the capture magnet obtained on sols 53 and 168 for an integration time of 10.3 hours: raw data (diamonds) with 11-point running mean (squares) and global fit (circles) as represented on Figure 7. The ^{210}Po and ^{244}Cm peaks are conspicuous. Source thickness between 1.5 and 3 μm explains the slight shift and the broadening of the ^{210}Po peak around channel 208. Channel 210–211 corresponds to the energy of alpha particles only attenuated by the 3 cm working distance through the Martian atmosphere. The ^{244}Cm signal is probably enhanced because the capture magnet has been targeted twice.

This expression is justified by the fact that both estimations of S + B are identical (only the estimation of B differs). After integration, even for the most critical case in terms of integration time (i.e., Capture magnet with second approach), S + B and B were large enough (42 and 204 counts, respectively) so the net signal, given by $(S + B)/t_{S+B} - B/t_B$, follows approximately a Gaussian distribution. Therefore the ±2σ confidence interval around the mean signal nearly corresponds to a 95% confidence interval.

[18] In order to convert the counting rates into surface activity, $A_s(^{210}\text{Po})$, in Bq cm^{-2}, the sensitivity of the instrument, Φ_{APXS}, with respect to a surface deposit of radionuclides has been derived analytically and numerically, using technical details provided by *Rieder et al.* [2003]. The instrument consists of a "ring" of 6 rectangular alpha detectors (13 × 7 mm) set out around the curium sources (Figure 9). The probability for an atom deposited on a targeted surface Σ to emit an alpha particle that is detected by the detector is:

$$f(P) = \eta_{\text{int}} \frac{\Omega(P)}{4\pi} \tag{3}$$

where η_{int} is the intrinsic efficiency of the detector and Ω(P) is the solid angle under which the detector is seen by the atom. Considering a circular geometry for both target and detector, with same axis, Ω(P) is given by

$$\Omega(\rho) = h. \int_0^{2\pi} \int_0^{b} \frac{r.dr.d\varphi}{(\rho^2 + h^2 + r^2 - 2.\rho.r.\cos(\varphi))^{3/2}} \tag{4}$$

where b is the radius of the detector and h its distance to the target. The flux of alpha particles detected, integrated over the whole surface Σ, is therefore (for a homogeneous source):

$$\begin{aligned}\Phi &= \int_{P\in\Sigma} f(P)\cdot dA_S(P) = \eta_{\text{int}} \cdot \int_{P\in\Sigma} \frac{\Omega(\rho)}{4\pi}\cdot A_S(P)\cdot\rho\cdot d\rho\cdot d\theta \\ &= \eta_{\text{int}} \cdot \frac{A_S}{2}\cdot \int_0^R \Omega(\rho).\rho.d\rho \end{aligned} \tag{5}$$

where $dA_S(P)$ is the activity of a surface element dS of Σ, $A_S(P)$ is the surface activity in Bq cm^{-2}, assumed to be constant, and R is the radius of the target. For the particular case of the APXS, a coefficient has to be included to compensate for the fact that the detector shape is not exactly a ring:

$$\Phi_{APXS} = \frac{S_{detectors}}{S_{ring}} \times \Phi_{ring} = \frac{S_{detectors}}{S_{ring}} \times (\Phi(b_1) - \Phi(b_2)) \tag{6}$$

After numerical integration, we finally find, assuming an intrinsic efficiency of 100%, and for R = 19 mm, b_1 = 21 mm, b_2 = 14 mm, h = 30 mm: Φ_{APXS} = 1.13 × 10^3 cph per Bq cm^{-2}.

[19] A numerical simulation with the multiparticles transport code MCNPX 2.4.0 [*MCNPX Team*, 2002; *Waters*, 2002] was also carried out. The six detectors were modeled by a silicon ring, of effective surface $(S_{\text{detectors}}/S_{\text{ring}}) \times S_{\text{ring}} = \alpha \times S_{\text{ring}} \approx 0.70 \times S_{\text{ring}}$, and the surface source of ^{210}Po consisted of a thin 19-mm diameter disk emitting alpha particles at 5.304 MeV, located in front of the detector head (filled with CO_2 at 2 × 10^{-5} g cm^{-3}), as described by *Rieder et al.* [2003]. This simulation gave the same result as the analytical approach. For the capture magnet, the target

Table 2. Quantitative Analysis of the ^{210}Po Signal[a]

	Gross Signal, cph		Blank, cph		Net Signal, cph		
	(S + B)	σ_{S+B}	(B)	σ_B	(S) = (S + B) − (B)	σ_S	Detection Threshold L_C, cph
First approach							
Soils + rocks	1.76	0.12	1.67	0.08	0.09	0.14	0.24
Capture magnet	4.10	0.63	1.72	0.08	2.38	0.64	0.69
Second approach							
Soils + rocks	1.76	0.12	1.61	0.11	0.15	0.16	0.28
Capture magnet	4.10	0.63	1.66	0.11	2.44	0.64	0.70
Mean net signal							
Soils + rocks					0.12	0.14	
Capture magnet					2.41	0.63	

[a]The "first approach" refers to the comparison between the gross signal and the background given by neighboring channels, fitted over the energy range [4.0 MeV–6.2 MeV]. The "second approach" refers to the comparison between the gross signal and the blank given by (RAT + trenches) spectra. Both net signals exceed the 95% detection threshold (95% critical level) [*Currie*, 1968]. The mean net signal is given with its standard deviation. Values are given in counts/hour (cph). The blank signal is slightly greater for the capture magnet because the center of the ^{210}Po peak was slightly shifted to lower energies (2 channels off).

has a reduced diameter (R = 12.5 mm), which leads to: $\Phi_{APXS} = 0.52 \times 10^3$ cph per Bq cm^{-2}.

[20] Consequently, the ^{210}Po activity measured on the capture magnet is: $A_s(^{210}\text{Po}) = 2.41/\Phi_{APXS} = 2.41/(0.52 \times 10^3) = (4.6 \pm 2.4) \times 10^{-3}$ Bq cm^{-2} (2σ confidence interval). On rocks and soils at the landing site, the surface activity of ^{210}Po could amount to 1.1×10^{-4} Bq cm^{-2}, but has an upper limit of $(S + 1.645 \times \sigma_s)/\Phi_{APXS} = (0.12 + 1.645 \times 0.14)/(1.13 \times 10^3) = 3.1 \times 10^{-4}$ Bq cm^{-2} (95% confidence level). The measured signal comes from the upper 1.5 μm of the surface layer. Indeed, by integrating the ^{210}Po signal over the range [5.15 MeV − 5.40 MeV], the target is probed over a depth of about 1.5 μm in a material of density 2.3 g cm^{-3}, a common figure for silicate minerals. However, this thickness is lower than the mean eolian dust particle diameter of 3 μm [*Lemmon et al.*, 2004]. Hence the integrated signal originates from ^{210}Po deposited on the upper half of the "visible" grains (thickness of 1.5 μm). For finer dust aggregates with bulk density 1.2 g cm^{-3}, the depth probed is roughly 3 μm. Over such thicknesses, the signal coming from the uranium-supported ^{210}Po is negligible.

3.2. Radon 222 Signal

[21] Opportunity's APXS also acquired atmospheric spectra on sols 7 and 79, for a total integration time of 18.5 hours. Integrating atmospheric spectra over the range [4.5 MeV–5.5 MeV] gives $(S + B) = 8.77$ cph with $\sigma_{S+B} = 0.69$ cph. Over the same range, the integration of the background spectrum (estimated from the fit) gives $B = 8.99$ cph with $\sigma_B = 0.20$ cph, yielding a detection threshold $L_C = 1.19$ cph. Hence $S = -0.22$ cph $< L_C$, meaning that there is no statistically significant difference between atmospheric and background spectra. Therefore results from atmospheric measurements are inconclusive. An upper limit of radon signal was found to be, at a 95% confidence level [*Currie*, 1968]: $S_{max} = 0 + 1.645 \times \sigma_s = 1.18$ cph.

[22] The geometrical sensitivity of the instrument with respect to a homogeneous volume distribution of ^{222}Rn (alpha emitter at 5.490 MeV) was derived numerically. It depends upon the source extent, i.e., the range of alpha particles considered, or the radius of the volume probed (in the present case, a portion of a sphere). Equivalently, this radius corresponds to a certain energy range. Since atmospheric spectra are contaminated by Rutherford Backscattering (RBS) on argon nuclei below channel 140, and RAT measurements by RBS on iron below channel 150, we integrated the spectrum over the range [4.5 MeV–5.5 MeV], to avoid any contamination. For a pressure of (7.5 ± 2) mbar and a temperature of 205K, this energy width corresponds to a working volume radius R of (0.7 ± 0.2) m, the distance over which a 5.5 MeV alpha particle loses 1 MeV [*Ziegler*, 2004]. We used the code MERCURE developed at the Commissariat à l'Energie Atomique (CEA) [*Suteau*, 2002], with its 3-D graphical interface MERCURAD, to determine the pure geometrical sensitivity of the detector (assuming that over this range, alpha particles move along straight lines). This code enables us to integrate the source volume by a Monte Carlo method and to calculate the direct flux at a given point of space. We considered a hemispheric volume source of radius R = 70 cm,

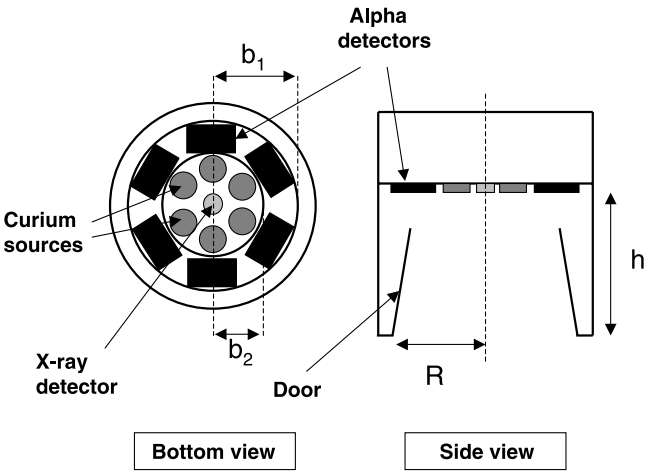

Figure 9. Simplified sketch of the APXS head [after *Rieder et al.*, 2003]. The alpha particle spectrometer consists of six rectangular detectors (7 × 13 mm) set out around six curium sources. The detection efficiency has been calculated using this simplified geometry (with R = 19 mm, b_1 = 21 mm, b_2 = 14 mm, h = 30 mm). The actual detection efficiency could be a little bit worse owing to the presence of the door and the source collimator (not depicted here) that slightly reduces the detector's field of view. A lower detection efficiency would yield a greater actual ^{210}Po activity.

and a cylindrical collimator with diameter 19 mm and depth 30 mm. The direct flux was calculated at different positions on the detector surface. The average value was then multiplied by the area of the 6 detectors. This simulation gave: Φ_{APXS} = 0.074 cph per Bq cm^{-3}. We also simulated the detector response with MCNPX 2.4.0. This transport code can calculate the energy deposited in a silicon chip and thus simulate an alpha spectra, taking into account not only the geometry of the source and detector, but also physical effects related to the transport of alpha particles in a volume filled with CO_2 (such as straggling and stopping power), which were not considered in the approach described previously. The detector response is obtained by integrating the spectrum simulated by MCNPX over the energy range of interest [4.5 MeV–5.5 MeV]. The geometry of the detector was the same as the one described above for the calculation of the sensitivity to a surface deposit of ^{210}Po. We found: Φ_{APXS} = 0.073 cph per Bq cm^{-3}.

[23] Consequently, an upper limit of radon activity at the landing site, $A_v(\mathrm{Rn})_{\max}$, was found to be, at a 95% confidence level: $A_v(\mathrm{Rn})_{\max} \approx 16 \pm 5$ Bq m^{-3}. It should be noted that at night, owing to strong temperature inversion [*Smith et al.*, 2004], radon is readily accumulated in the boundary layer around its emission zone [*Sabroux et al.*, 2003]. This upper limit, obtained at nighttime, is therefore mostly representative of local conditions at the landing site, where the exhalation rate is not expected to be very large because the regolith at Meridiani Planum is no more than 1 or 2 meters thick [*Squyres et al.*, 2004].

3.3. Possible Presence of a ^{218}Po Signal

[24] The presence of two peaks above the 2σ detection threshold on Figure 1d around channel 239–240 is worth discussing. These two peaks, together with the ^{244}Cm anomaly, explain the presence of a negative peak centered halfway on Figure 5d, above the 97.5% detection threshold. Because we are considering a data set of almost hundred points, this peak may stem from pure statistical fluctuations (this also holds for the peak at channel 210, but with a probability less than 2.5%, since we are considering a specific channel). However, any ^{218}Po signal attenuated by 3 cm of CO_2 would produce a peak centered at channel 242 ± 1.5 according to the global energy calibration that we derived, and precisely at channel 239, according to a more local energy calibration (see Energy calibration of APXS spectra). Therefore we put forward another possible and meaningful explanation: following an hours-long abrasion by the Rock Abrasion Tool, the sampled surfaces get charged by triboelectricity, as confirmed by the presence of fine-grained abraded material that was observed on several RAT targets after it fell into the borehole (as imaged, for instance, by Spirit Microscopic Imager on target "Clovis" on sol 217). Charged surfaces can act as efficient ^{218}Po aerosols collectors, since ^{218}Po atoms are electrically charged following their formation. As a result, alpha spectra would be contaminated by ^{218}Po on abraded surfaces only (Figure 1d around channel 239). As a matter of fact, this process is sometimes used to collect ^{218}Po and measure its concentration [*Khan and Phillips*, 1985]. For a hypothetical radon activity of 10 Bq m^{-3}, the collection of a volume of 1 liter (or half a sphere of 5 cm radius) filled with ^{218}Po in equilibrium with ^{222}Rn would be sufficient to account for the measured net signal. Some lab experiments at low pressure and under dry conditions would be needed to test this hypothesis. This value of 10 Bq m^{-3} is consistent with the measured ^{210}Po signal and upper limit of ^{222}Rn: it is below the latter (<16 Bq m^{-3}) but might be reached at night in the first meter of the boundary layer under very strong temperature inversion if the exhalation rate is taken equal to the inferred global exhalation rate of 5–10 × 10^{-3} atoms cm^{-2} s^{-1} (see section 4).

4. Discussion

[25] The amount of ^{210}Po present on the surface depends upon the amount of ^{222}Rn released from the ground during the last few decades. The time delay between ^{222}Rn exhalation and ^{210}Po disintegration is constrained by the 22.3 years half-life of ^{210}Pb, which is deposited on the ground with dust, minus a fraction that is airborne (after possible multiple deposition and resuspension). A simple box model of atmospheric and ground reservoirs of radon and its progeny, similar to the one detailed by *Lambert et al.* [1982] for the Earth and depicted in Figure 2, yields, at steady state and without considering the uranium-supported ^{210}Po activity:

$$A_{total}(^{210}\mathrm{Po}) = A_{surf}(^{210}\mathrm{Po}) + A_{atmo}(^{210}\mathrm{Po}) = \Phi_{\mathrm{Rn}} + \Phi^{*}_{\mathrm{Rn}} = A_{atmo}(^{222}\mathrm{Rn}) + \Phi^{*}_{\mathrm{Rn}} \quad (7)$$

where $A_{surf}(^{210}\mathrm{Po})$ is the surface activity of ^{210}Po, integrated over the depth of the surface layer regularly mobilized by winds – or over the depth of accumulation of young (<100 yr) eolian deposits, if there is net accumulation; $A_{atmo}(^{210}\mathrm{Po})$ represents the activity of the atmospheric ^{210}Po reservoir, carried by dust; $A_{atmo}(^{222}\mathrm{Rn})$ is the total atmospheric radon activity; Φ_{Rn} is the radon exhalation rate and Φ^{*}_{Rn} the radon flux from underground that is adsorbed at night in the coldest upper centimeters of the soil and that disintegrates before being released into the atmosphere (Φ^{*}_{Rn}= 0 on Earth, but not on the Moon [*Lambert et al.*, 1977]). Therefore, if the ^{210}Po radioactivity of the dust is measured, the knowledge of both the atmospheric dust loading and the thickness of the surface layer which is regularly recycled can yield $A_{atmo}(^{210}\mathrm{Po})$ and $A_{surf}(^{210}\mathrm{Po})$, and thus provide an estimate of the global average radon exhalation rate. Over the depth that we considered (<3 μm), there is no significant contribution from Φ^{*}_{Rn}. Indeed, Φ^{*}_{Rn}, trapped at night, could lead to an enrichment of unsupported ^{210}Po in the first few centimeters of the regolith (which correspond to the diurnal thermal skin depth), while the enrichment in ^{210}Po of atmospheric dust particles stemming from the term Φ_{Rn} is concentrated over a thickness of a few microns only. Therefore, over the first few microns, the contribution from Φ^{*}_{Rn} is negligible as compared to the one from Φ_{Rn} and our estimate of the integrated activity (to be discussed later) really gives an estimate of Φ_{Rn}.

[26] On Mars, the frequent occurrence of regional and global dust storms, as well as the widespread dust devils activity, have most likely homogenized the dust particles with respect to their ^{210}Pb content, deposited on particles surface during their atmospheric transport. Therefore one expects the profile of ^{210}Pb (and thus of ^{210}Po, supposed to

be in secular equilibrium with its parent) to be constant throughout the depth of the reworked surface layer, over most of the planet's surface (all the more so if this layer is thin). This profile is rather decreasing with depth in regions where there is net deposition of dust, without resuspension, as observed on Earth in undisturbed soils [*Matisoff et al.*, 2002], but this is expected only in regions of Mars that have been permanent sinks of dust over the last century, such as the northern residual polar cap [*Pollack et al.*, 1979].

[27] Capture magnets represent an ideal target, because we can directly measure the ^{210}Po-induced radioactivity of the dust. Moreover, this dust sample is rather representative of the Martian aerosol, since essentially all the dust suspended in the Martian atmosphere is somewhat magnetic, according to *Leer et al.* [2004] and *Bertelsen et al.* [2005], and because the capture magnet was designed to attract all magnetic dust particles within its reach [*Madsen et al.*, 2003; *Leer et al.*, 2004]. Spectra acquired on the filter magnet before sol 54 could not be analysed because of a drift in calibration.

[28] On the Moon, unsupported ^{210}Po originating from exhalated radon has accumulated over a depth of no more than 1 μm [*Gorenstein and Bjorkholm*, 1972]. Measurements of ^{222}Rn and ^{210}Po by Surveyor 5, 6 and 7 [*Turkevich et al.*, 1970], mapping by the Apollo 15, 16 [*Bjorkholm et al.*, 1973; *Gorenstein and Bjorkholm*, 1973] and the Lunar Prospector [*Lawson et al.*, 2005] missions, as well as analysis of returned samples [*Grjebine et al.*, 1972], revealed temporal variations and large disparities in their spatial distribution. These were explained by the presence of active degassing spots [*Gorenstein and Bjorkholm*, 1973; *Friesen and Adams*, 1976], of time-variable degassing intensities [*Lawson et al.*, 2005]. Lunar Prospector mapped a few areas with ^{210}Po activities of the order of 2 to 4 $\times$ 10^{-2} Bq cm^{-2} [*Lawson et al.*, 2005]. However, in order to draw comparisons between exhalation rates on a global and long-term scale, it is preferable to use spatially averaged quantities. Indeed, this integrates simultaneously time and space variations, and the different processes involved – namely, exhalation through diffusion over most of the planet surface and intermittent venting events in a few locations. An average surface activity of ^{210}Po of (1.5 ± 0.4) $\times$ 10^{-3} Bq cm^{-2} was measured by the alpha spectrometers onboard Apollo 15 and 16 orbiting modules [*Bjorkholm et al.*, 1973].

[29] On Mars, a good estimate of the depth of the dust reservoir that is recycled on a regular basis is given by the global dust mass loading observed during dust storm seasons. The global dust mass loading of the atmosphere as measured by the Mars Orbiter Camera (MOC) in 1999 accounts for an equivalent depth of 2.6 to 4.0 μm [*Cantor et al.*, 2001], for a bulk soil density of 1 g cm^{-3}. Hence, according to the ^{210}Po radioactivity measured by the APXS, and assuming an average depth of 3.3 μm, A_{total}(^{210}Po) is comprised between 5.1 (±2.6) and 10.1 (±5.3) $\times$ 10^{-3} Bq cm^{-2}, depending on the depth probed (1.5 to 3 μm). This is greater than the lunar value by a factor of 3.4 to 6.7. Furthermore, the mass loading measured by MOC was found to be 6–8 times lower than the global storm mass loading of 1977, so A_{total}(^{210}Po) could be even greater.

[30] On the Moon, even though the escape ratio of ^{218}Po is known (= 0.5), the disequilibrium factor that would correspond to a steady state between ^{210}Po and ^{222}Rn is not accurately known because of uncertain escape ratios of the intermediate isotopes ^{214}Pb and ^{210}Pb (nonetheless, these can be shown to be less than 0.3 and 0.2 by pure geometrical considerations based on the range of the recoiling atoms, the most critical case corresponding to a surface perfectly smooth and planar, which is not realistic). On Mars, however, because there is no escape of radon daughters to space, equation (7) fully applies, and we can infer from ^{210}Po measurements that the global average radon flux is comprised between 5.1 and 10.1 $\times$ 10^{-3} atom cm^{-2} s^{-1}. Apollo 15's alpha particles spectrometer measured an average radon activity, A_{atmo}(^{222}Rn), of at most $\sim$1 $\times$ 10^{-3} Bq cm^{-2} [*Gorenstein and Bjorkholm*, 1972, 1973], corresponding to an average flux of $\sim$1 $\times$ 10^{-3} atom cm^{-2} s^{-1}, which is 5 to 10 times lower than the Martian value. Therefore we conclude that both the global average ^{210}Po surface activity and ^{222}Rn flux are larger on Mars than on the Moon.

[31] This means that a comparatively more efficient process enables radon to leave the ground. This process should be even more efficient if it was to compensate for a somewhat lower thorium (hence, most likely, uranium) content of the Martian soil, as shown by Mars Odyssey GRS and Lunar Prospector measurements [*Lawrence et al.*, 2003; *Warren*, 2005; *Gillis et al.*, 2004; *Taylor et al.*, 2004]. Possible reasons for a higher exhalation rate of radon are (1) less extreme temperatures at night, which create an impermeable cap at the surface of the Moon because of strong adsorption [*Lambert et al.*, 1975], even though the mean ground temperature is lower on Mars (210 K) than on the Moon (250 K); (2) molecular diffusion and advection are possible in the large pores of the regolith, whereas the lunar regolith is under vacuum conditions, under which radon transport is controlled by pure Knudsen diffusion [*Friesen and Adams*, 1976]; and (3) at same temperature, less efficient adsorption on Mars regolith owing to the presence of other absorbable gases, such as carbon dioxide and water vapor. These mechanisms enhance radon transport ability and exhalation, but not its emanation rate. *Sabroux et al.* [2003, 2004] suggested that the presence of water ice in the first meters of the subsurface, in unsaturated zones of the midlatitude regions, could lead to a very significant increase of radon emanation rate.

[32] The presence of ^{210}Po in rock varnish has been measured in arid regions on Earth [*Fleisher et al.*, 1999; *Hodge et al.*, 2005]. These authors have concluded that this isotope, in secular equilibrium with its parent ^{210}Pb, was extracted from the atmosphere, and that virtually any surface in arid regions exposed to the atmosphere would exhibit a noticeable ^{210}Po alpha activity. It is worth comparing their values with the value measured on Martian rocks. Even though the activity measured on rocks and soils is lower than the 95% detection threshold, it is interesting to consider the net signal as a rough estimate (1.1 $\times$ 10^{-4} Bq cm^{-2} over $\sim$1.5 μm). *Hodge et al.* [2005] reported a surface activity of 0.035 ± 0.015 Bq cm^{-2} on rocks collected in Nevada, integrated over a depth of 5 μm. This yields a Mars/Earth ratio of about 0.01. According to the box model that we used, we can infer a radon flux on Mars of 5–10 $\times$ 10^{-3} atoms cm^{-2} s^{-1}. The average radon flux on the global Earth (including oceans) is about 0.3 atoms cm^{-2} s^{-1}, which yields a Mars/Earth ratio of 0.017–0.033, a figure of the same magnitude. Several

explanations can account for the difference between both planets, Mars being characterized by: (1) a lower crustal uranium content, (2) a drier soil, which reduces the emanation factor, and (3) a much stronger adsorption on the soil matrix. Further studies are needed to fully characterize the competing effects of adsorption, emanation's increase with water ice (in unsaturated soils only) and enhanced molecular diffusion (in contrast to the lunar soil, gas transport in the Martian soil is in a transport regime between Knudsen and molecular diffusion).

5. Conclusions

[33] Although the APXS of MER rovers was not specifically designed for this purpose, the energy bandwidth of the alpha detectors was large enough to cover the energy range of alpha particles emitted by some natural radioactive isotopes of the ^{238}U series. A differential statistical analysis of alpha spectra revealed the presence of ^{210}Po on Martian dust at the landing site, providing indirect evidence for the presence of radon in the Martian atmosphere. The dust ^{210}Po activity of $(4.6 \pm 2.4) \times 10^{-3}$ Bq cm^{-2}, measured over a depth of 1.5 to 3 μm on the dust magnet, allows comparison with the Earth and the Moon. Indeed, on Mars, because of the long half-life of ^{210}Pb, the low net production of aerosols over timescales of a few decades and because of the existence of frequent and global dust mobilization processes, one can reasonably assume that the ^{210}Po activity of the dust surface layer stirred up by winds is homogeneously distributed. As a result, variations are not expected to be as wide as on the Moon, and a local measurement of the dust ^{210}Po radioactivity is sufficient to provide an estimate of the global average ^{222}Rn exhalation rate if the load of this dust reservoir can be estimated. Radon 222 itself has not been detected directly. A longer integration time on atmospheric targets and a better geometrical detection efficiency would have been necessary to measure it.

[34] Combined with Gamma Ray Spectrometer surficial radioactivity mapping and in situ meteorological data, the measurement of radon and its decay products can provide valuable information on important geological properties of the regolith, including its water content, as well as on gaseous and particulate matter surface exchange processes, and recent outgassing events, as sought on the Moon since the 1960s. A better knowledge of the depth of the surface layer reworked over the last century would yield a better estimate of the global average radon exhalation rate. Conversely, a simultaneous measurement of atmospheric ^{222}Rn and surface ^{210}Po would allow to estimate this thickness and thus better understand surface recycling processes on Mars. This strongly advocates the development of a dedicated instrument for radon measurement in the Mars boundary layer. Results obtained so far with Opportunity's APXS pave the way for designing such an instrument.

[35] **Acknowledgments.** We thank R. Gellert for crucial information on the design and operation of MER APXS and for fruitful discussions and comments. We are grateful to J. C. Le Roulley for his expertise on lunar radon and to P. Blanchis and P. Richon for helpful insights on alpha spectroscopy and data analysis. This paper benefited from an in-depth review by D. J. Lawrence and anonymous referees. The present investigation was carried out within the framework of a Ph.D. research thesis cofunded by the French Space Agency CNES (Centre National d'Etudes Spatiales).

References

Bertelsen, P., et al. (2004), Magnetic properties experiments on the Mars Exploration Rover Spirit at Gusev Crater, *Science*, *305*, 827–829.

Bertelsen, P., et al. (2005), Dynamic dust accumulation and dust removal observed on the Mars Exploration Rover magnets, *Proc. Lunar Planet. Sci. Conf., 36th*, Abstract 2250.

Bjorkholm, P., L. Golub, and P. Gorenstein (1973), Detection of nonuniform distribution of polonium-210 on the Moon with the Apollo 16 alpha particle spectrometer, *Science*, *180*, 957–959.

Cantor, B. A., P. B. James, M. Caplinger, and M. J. Wolff (2001), Martian dust storms: 1999 Mars Orbiter Camera observations, *J. Geophys. Res.*, *106*(E10), 23,653–23,687.

Catling, D. C. (2005), Twin studies on Mars, *Nature*, *436*, 42–43.

Currie, L. A. (1968), Limits for qualitative detection and quantitative determination: Application to radiochemistry, *Anal. Chem.*, *40*, 586–593.

Fleisher, M., T. Liu, W. S. Broecker, and W. Moore (1999), A clue regarding the origin of rock varnish, *Geophys. Res. Lett.*, *26*, 103–105.

Friesen, L. J., and J. A. S. Adams (1976), Low pressure radon diffusion—A laboratory study and its implications for lunar venting, *Geochim. Cosmochim. Acta*, *40*, 375–380.

Gellert, R., et al. (2004), Chemistry of rocks and soils in Gusev Crater from the alpha particle X-ray spectrometer, *Science*, *305*, 829–832.

Gillis, J. J., B. L. Jolliff, and R. L. Korotev (2004), Lunar surface geochemistry: Global concentrations of Th, K, and FeO as derived from Lunar Prospector and Clementine data, *Geochim. Cosmochim. Acta*, *68*, 3791–3805.

Gorenstein, P., and P. Bjorkholm (1972), Observation of lunar emanation with the Apollo 15 alpha particle spectrometer, *Proc. Lunar Sci. Conf. 3rd, Geochim. Cosmochim. Acta*, *3*, suppl. 3, 2179–2187.

Gorenstein, P., and P. Bjorkholm (1973), Detection of radon emanation from the crater Aristarchus by the Apollo 15 alpha particle spectrometer, *Science*, *179*, 792–794.

Grjebine, T., G. Lambert, and J. C. Le Roulley (1972), Alpha spectrometry of a surface exposed lunar rock, *Earth Planet. Sci. Lett.*, *14*, 322–324.

Hodge, V. F., D. E. Farmer, T. Diaz, and R. L. Orndorff (2005), Prompt detection of alpha particles from ^{210}Po: Another clue to the origin of rock varnish?, *J. Environ. Radioact.*, *78*, 331–342.

Khan, A., and C. R. Phillips (1985), Dependence of electrostatic diffusion of Rn progeny on environmental parameters, *Health Phys.*, *49*, 443–454.

Lambert, G., J. C. Le Roulley, and P. Bristeau (1975), Evidence of gaseous radon-222 between fines grains within lunar regolith, *Proc. Lunar Sci. Conf., 6th*, 1803–1809.

Lambert, G., J. C. Le Roulley, and P. Bristeau (1977), Accumulation and circulation of gaseous radon between lunar fines, *Philos. Trans. R. Soc. London, Ser. A.*, *285*, 331–336.

Lambert, G., G. Polian, J. Sanak, B. Ardouin, A. Buisson, A. Jegou, and J. C. Le Roulley (1982), The radon cycle and its daughters: An application to the study of troposphere-stratosphere exchanges, *Ann. Geophys.*, *38*, 497–531.

Lawrence, D. J., R. C. Elphic, W. C. Feldman, T. H. Prettyman, O. Gasnault, and S. Maurice (2003), Small area thorium features on the lunar surface, *J. Geophys. Res.*, *108*(E9), 5102, doi:10.1029/2003JE002050.

Lawson, S. L., W. C. Feldman, D. J. Lawrence, K. R. Moore, R. C. Elphic, R. D. Belian, and S. Maurice (2005), Recent outgassing from the lunar surface: The Lunar Prospector alpha particle spectrometer, *J. Geophys. Res.*, *110*, E09009, doi:10.1029/2005JE002433.

Leer, K., J. I. Hjollum, P. Bertelsen, W. Goetz, K. Kinch, S. F. Hviid, J. Knudsen, and M. B. Madsen (2004), Magnetic properties of dust on Mars—Results from the Mars Exploration Rovers, *Eos Trans. AGU*, *85*(47), Fall Meeting Suppl, Abstract P21A-0200.

Lemmon, M. T., et al. (2004), Atmospheric imaging results from the Mars Exploration Rovers: Spirit and Opportunity, *Science*, *306*, 1753–1756.

Madsen, M. B., et al. (2003), Magnetic properties experiments on the Mars Exploration Rover mission, *J. Geophys. Res.*, *108*(E12), 8069, doi:10.1029/2002JE002029.

Matisoff, G., E. C. Bonniwell, and P. J. Whiting (2002), Soil erosion and sediment sources in an Ohio watershed using beryllium-7, Cesium-137, and Lead-210, *J. Environ. Qual.*, *31*, 54–61.

Mayer, M. (1997), SIMNRA user's guide, *Rep. IPP 9/113,* Max-Planck-Inst. für Plasmaphys., Garching, Germany.

MCNPX Team (2002), MCNPX, version 2.4.0, *Rep. LA-UR-02-5253*, Los Alamos Natl. Lab., Los Alamos, N. M.

Pollack, J. B., D. S. Colburn, F. M. Flasar, R. Kahn, C. E. Carlston, and D. G. Pidek (1979), Properties and effects of dust particles suspended in the Martian atmosphere, *J. Geophys. Res.*, *84*, 2929–2945.

Rieder, R., and R. Gellert (2004), MER 1 alpha particle X-Ray spectrometer 2 EDR V1.0, *Data Set MER1-M-APXS-2-EDR-OPS-V1.0,* http://starbrite.jpl.nasa.gov/pds/viewProfile.jsp?dsid=MER1-M-APXS-2-EDR-OPS-V1.0, NASA Planet. Data Syst., Greenbelt, Md.

Rieder, R., H. Wänke, T. Economou, and A. Turkevich (1997), Determination of the chemical composition of Martian soil and rocks: The alpha proton X ray spectrometer, *J. Geophys. Res.*, *102*(E2), 4027–4044.

Rieder, R., R. Gellert, J. Brückner, G. Klingelhöfer, G. Dreibus, A. Yen, and S. W. Squyres (2003), The new Athena alpha particle X-ray spectrometer for the Mars Exploration Rovers, *J. Geophys. Res.*, *108*(E12), 8066, doi:10.1029/2003JE002150.

Rieder, R., et al. (2004), Chemistry of rocks and soils at Meridiani Planum from the alpha particle X-ray spectrometer, *Science*, *306*, 1746–1749.

Ruff, S. W., and P. R. Christensen (2002), Bright and dark region on Mars: Particle size and mineralogical characteristics based on Thermal Emission Spectrometer data, *J. Geophys. Res.*, *107*(E12), 5127, doi:10.1029/2001JE001580.

Sabroux, J. C., N. Michielsen, V. Voisin, C. Ferry, P. Richon, J. F. Pineau, J. C. Le Roulley, and E. Chassefière (2003), Paloma-radon: Atmospheric radon-222 as a geochemical probe for water in the Martian subsoil, *Geophys. Res. Abstr.*, *5*, Abstract 12690.

Sabroux, J. C., N. Michielsen, V. Voisin, C. Ferry, P. Richon, and J. F. Pineau (2004), NITON: A new geophysical tool based on atmospheric radon for water exploration in the Martian soil, *Geophys. Res. Abstr.*, *6*, Abstract 07770.

Smith, M. D., et al. (2004), First atmospheric science results from the Mars Exploration Rovers Mini-TES, *Science*, *306*, 1750–1753.

Soderblom, L. A., et al. (2004), Soils of Eagle Crater and Meridiani Planum at the Opportunity Rover landing site, *Science*, *306*, 1723–1726.

Soong, T. T. (2004), *Fundamentals of Probability and Statistics for Engineers*, 406 pp., John Wiley, Hoboken, N. J.

Squyres, S. W., et al. (2004), The Opportunity Rover's Athena science investigation at Meridiani Planum, Mars, *Science*, *306*, 1698–1703.

Strom, D. J., and J. A. MacLellan (2001), Evaluation of eight decision rules for low-level radioactivity counting, *Health Phys.*, *81*(1), 27–34.

Suteau, C. (2002), Code MERCURE-6.1. Code de propagation des photons par la méthode d'atténuation en ligne droite: Notice de principe, *CEA Rep. SERMA/LEPP/RT/02-3066/A*, Comm. à l'Energie At., Paris.

Taylor, G. J., W. Boynton, H. Wänke, G. Dreibus, and J. Brückner (2004), Using Mars Odyssey GRS data to assess models for the bulk composition of Mars, *Proc. Lunar Planet. Sci. Conf., 35th*, Abstract 1808.

Turkevich, A. L., J. H. Patterson, E. J. Franzgrote, K. P. Sowinski, and T. E. Economou (1970), Alpha radioactivity of the lunar surface at the landing sites of Surveyors 5, 6, and 7, *Science*, *167*, 1722–1724.

Warren, P. H. (2005), "New" lunar meteorites: Implications for composition of the global lunar surface, lunar crust, and the bulk Moon, *Meteorit. Planet. Sci.*, *40*, 477–506.

Waters, L. S. (2002), MCNPX user's manual, version 2.4.0, *Rep. LA-CP-02-408*, Los Alamos Natl. Lab., Los Alamos, N. M.

Ziegler, J. F. (2004), SRIM-2003, *Nucl. Instrum. Methods Phys., Sect. B*, *219*, 1027–1036.

L. Berger, P.-Y. Meslin, and J.-C. Sabroux, IRSN, Centre de Saclay, B.P. 68, F-91192 Gif-sur-Yvette, France. (pierre-yves.meslin@irsn.fr)

E. Chassefière, Service d'Aéronomie, IPSL, Aile 45-46, 4ème étage, boîte 102, 4 place Jussieu, F-75252 Paris, France.

J.-F. Pineau, ALBEDO Technologies, Route de St Pardoux, F-87640 Razès, France.